

Improved Photometric Redshifts with Surface Luminosity Priors

Lifang Xia¹, Seth Cohen¹, Sangeeta Malhotra¹, James Rhoads¹, Norman Grogin¹, Nimish P. Hathi², Rogier A. Windhorst¹, Nor Pirzkal³, Chun Xu³

ABSTRACT

We apply Bayesian statistics with prior probabilities of galaxy surface luminosity (SL) to improve photometric redshifts. We apply the method to a sample of 1266 galaxies with spectroscopic redshifts in the GOODS North and South fields at $0.1 \lesssim z \lesssim 2.0$. We start with spectrophotometric redshifts (SPZs) based on Probing Evolution and Reionization Spectroscopically grism spectra, which cover a wavelength range of 6000–9000Å, combined with $(U)BViz(JHK)$ broadband photometry in the GOODS fields. The accuracy of SPZ redshifts is estimated to be $\sigma(\Delta(z)) = 0.035$ with an systematic offset of -0.026 , where $\Delta(z) = \Delta z / (1 + z)$, for galaxies in redshift range of $0.5 \lesssim z \lesssim 1.25$. The addition of the SL prior probability helps break the degeneracy of SPZ redshifts between low redshift 4000 Å break galaxies and high-redshift Lyman break galaxies which are mostly catastrophic outliers. For the 1138 galaxies at $z \lesssim 1.6$, the fraction of galaxies with redshift deviation $\Delta(z) > 0.2$ is reduced from 15.0% to 10.4%, while the rms scatter of the fractional redshift error does not change much.

Subject headings: Method: Bayesian Statistic - Prior Probability - Galaxies: Photometric Redshift - Surface Luminosity

1. Introduction

In recent years, the technique of photometric redshift has been widely used to determine redshifts of galaxies for large imaging sky surveys (e.g., Wolf et al. 2003; Mobasher et al. 2004, 2007). This technique is useful for redshift estimation of large numbers of faint galaxies at high redshift which are currently too faint for spectroscopy. There are typically two methods of redshift estimation by broadband photometry. One approach is an empirical

¹School of Earth and Space Exploration, Arizona State University, AZ, 85287-1404; lifang.xia@asu.edu

²Department of Physics and Astronomy, University of California, Riverside, CA, 92521

³Space Telescope Science Institute, Baltimore, MD, 21218

method, which calibrates an empirical training relation between photometric magnitudes or colors and galaxy spectroscopic redshifts, and applies it to the observed photometric sample (Connolly et al. 1995; Wang et al. 1999). Another approach is a template spectral energy distribution (SED) fitting method, which obtains best-fit redshifts by comparing the observed SEDs to that of a large empirical or model template library (Baum 1962; Koo 1985; Fernández-Soto et al. 1999; Bolzonella et al. 2000; Budavári et al. 1999, 2000, 2001; Csabai et al. 2000; Wolf et al. 2001; Blanton et al. 2003). The efficiency of SED fitting is based on fitting the overall shape of spectra, the detection of strong spectral properties, such as the 4000Å/Balmer break and Lyman break, and the amount of dust present in red galaxies.

The general accuracy of photometric redshift ranges from $\sigma_z = 0.02$ to 0.05, which strongly depends on the number of filters and other factors, such as the precision of the photometry, the zero points, the image FWHM, and of course the quality of the templates and the fitting code. Hickson et al. (1994) show that the redshift accuracy by SED fitting is comparable to slitless spectroscopy from a simulation of 40 band photometry. Practical multicolor sky surveys, such as the Classifying Objects by Medium-Band Observations (COMBO)-17 survey, using 17 intermediate-band filters (Wolf et al. 2003) and the Beijing-Arizona-Taipei-Connecticut (BATC) sky survey, using 15 intermediate-band filters, achieve a typical accuracy of $\sigma_z = 0.02$ for photometric redshift estimation (Zhou et al. 2001; Xia et al. 2002). The photometric redshift accuracy using by five broadband filters is about 0.05 (Blanton et al. 2003). However, the depth of intermediate-band sky surveys are generally constrained to $z < 0.1$, and the observations of multiple bands can be quite time consuming. Broadband photometry has the advantage of sensitivity which enables photometric redshifts of large samples of faint and high redshift galaxies. The photometric redshifts from broadband fluxes tend to have large dispersion and strong degeneracy between low-redshift Balmer break galaxies and high-redshift Lyman break galaxies, which leads to the degeneracy of the photometric redshift estimation.

To break such degeneracies, Benítez (2000) developed a Bayesian method of photometric redshift estimation (BPZ) using galaxy magnitudes as Bayesian priors. This method produced an accuracy of $\sigma(\Delta(z)) \approx 0.06$, where $\Delta(z) = \frac{\Delta z}{1+z}$, for galaxies in Hubble Deep Field North (HDF-N) up to $z < 6$. Mobasher et al. (2007) estimate redshifts for galaxies at $z < 1.2$ with 16 bands photometry from 3500 to 23000 Å by different photometric redshift codes with and without luminosity function (LF) priors. The results give an accuracy of $\sigma(\Delta(z)) \approx 0.031$ and find slight improvement in the redshift estimation with LF priors.

Observed galaxy surface brightness is a promising observational parameter to break the redshift degeneracy (Koo 1999). Tolman (1930) first showed that the surface brightness

dims with redshift as $(1+z)^{-4}$ in an expanding universe independent of the cosmology. With this sensitive a dependence on $(1+z)$, surface brightness should make a good prior for the redshift estimation. The only caveat is the evolution of intrinsic galaxy luminosity per area with redshift. Passive evolution of stellar populations leads to a significant brightening of intrinsic luminosities per unit area at higher redshifts (Pahre et al. 1996; Sandage & Lubin 2001) and therefore to a less steep surface brightness redshift relation.

Using surface brightness priors, Kurtz et al. (2007) provide a redshift estimator by taking the median redshift in small bins in galaxy surface brightness-color space. The estimator is applied to the 10%-20% reddest galaxies from the Smithsonian Hectospec Lensing survey (SHELS), and achieves an accuracy of $\sigma(\Delta(z)) = 0.025$ for $z < 0.8$. ?) use the five-band Sloan Digital Sky Survey (SDSS) photometry, surface brightness and the Sérsic index to provide improved photometric redshifts in SDSS. They apply seven-dimensional probability arrays for spectroscopically confirmed galaxies at $z < 0.25$, which yields $\sigma(\Delta(z)) = 0.025$ for red galaxies and 0.03 for blue galaxies. Stabenau et al. (2008) apply surface brightness priors to ground based VIMOS VLT Deep Survey (VVDS) and the space-based GOODS (Giavalisco et al. 2004) field from Hubble Space Telescope (HST), and improve the bias and scatter by a factor of 2 for galaxies in the range $0.4 < z < 1.3$ to get a scatter of $\sigma(\Delta(z)) \approx 0.08$. In this paper, we use spectrophotometric redshifts (SPZs) which use low-resolution grism data and broadband data in the GOODS fields as our starting point (Ryan et al. 2007; Cohen et al. 2009, in preparation). The SPZs have a scatter in $\sigma(\Delta(z)) \approx 0.03$. We then use color and surface brightness priors, which we adopt the unit of luminosity per area (Hathi et al. 2008), L_{\odot}/kpc^2 , and hereafter we call it surface luminosity (SL) priors, to break the redshift degeneracy to derive photometric redshifts for a sample of 1266 galaxies in the GOODS North (GOODS-N) and South (GOODS-S) fields with spectroscopic redshifts between $0.1 \lesssim z \lesssim 2.0$.

This paper is organized as follows. We briefly describe the observations, the data, and the result of the spectrophotometric redshift estimation in Section 2 . The application of color and SL priors is given in Section 3. The results of redshift estimation with hybrid of SPZ and surface luminosity priors are illustrated in Section 4. Finally, we discuss our results and present our conclusions in Section 5. Throughout this paper, we assume a Λ CDM cosmological model with matter density $\Omega_m = 0.28$, vacuum density $\Omega_{\Lambda} = 0.72$, and Hubble constant $H_0 = 100h \text{ km s}^{-1} \text{ Mpc}^{-1}$, with $h = 0.7$ for the calculation of distances (Komatsu et al. 2009).

2. Observation and Data

We select a sample of 1266 galaxies in GOODS-N and GOODS-S fields which have both spectroscopic (Wirth et al. 2004; Grazian et al. 2006; Vanzella et al. 2008) and spectrophotometric redshifts (Cohen et al. 2009, in preparation) to test the application of SL priors. Only spectroscopic redshifts with quality flag $Q = 0$, or 1 (0: very good quality, 1: good quality) are used. These galaxies have both grism spectra, from the *HST*/Advanced Camera for Survey (ACS Ford et al. 2003) Probing Evolution and Reionization Spectroscopically (PEARS; S. Malhotra, PI) survey, and optical broadband $BViz$ photometry from *HST*/ACS GOODS version 2.0 images (Giavalisco et al. 2004). The ACS grism spectra cover a wavelength range from 6000 to 9000 Å (Pirzkal et al. 2004) for objects in parts of the GOODS-N and GOODS-S fields. The galaxies in our PEARS sample are located in four ACS pointings in the GOODS-N and GOODS-S fields. The photometry in the GOODS-N field is supplemented with ground-based U -band data from Capak et al. (2004), and photometry in the GOODS-S field is supplemented with the JHK -band data from VLT ESO/GOODS project (Retzlaff et al. 2009, in preparation). The photometry and the aperture correction between the broad-band data are described in detail by Ryan et al. (2007) and Cohen et al. (2009, in preparation). Figure 1 shows the histogram of the distribution of galaxy spectroscopic redshifts. The redshifts of most galaxies are less than $z \sim 2.0$. The final sample of 1266 galaxies are selected with spectroscopic redshifts in the range of $0.1 \lesssim z \lesssim 2.0$.

The SPZs (Ryan et al. 2007; Cohen et al. 2009, in preparation) are estimated based on the SED fitting of the combination of grism spectra and UV–optical–infrared broadband photometry by the photometric redshift code *HyperZ* (Bolzonella et al. 2000). The SPZ method achieves a redshift accuracy of $\sigma(\Delta(z)) = 0.035$ for the 465 galaxies in the GOODS-N field at redshift range $0.5 \lesssim z \lesssim 1.25$ with a catastrophic outlier fraction of 18.2%. The catastrophic outliers are defined as galaxies with fractional redshift errors, $\Delta(z)$, greater than 3σ of the rms scatter in the sample. The best accuracy of the SPZ method is achieved for the redshift range $0.5 \lesssim z \lesssim 1.25$, where the 4000Å break falls in the peak sensitivity wavelength range of the ACS grism. The redshifts estimated by SPZ tend to show a strong redshift degeneracy. This is demonstrated in the upper panels of Figure 6, which compare SPZ redshifts with spectroscopic redshifts. A substantial fraction of galaxies at $z < 0.6$ scatter to $SPZ \simeq 2 - 3$. To improve the redshift accuracy of the SPZ redshift estimation, we apply the prior probability of galaxy SL to constrain and break the degeneracy, since surface brightness is tightly related to redshift as approximately $(1+z)^{-4}$ for bolometric fluxes and $(1+z)^{-(4+\alpha)}$ for fluxes per unit frequency (Tolman 1930).

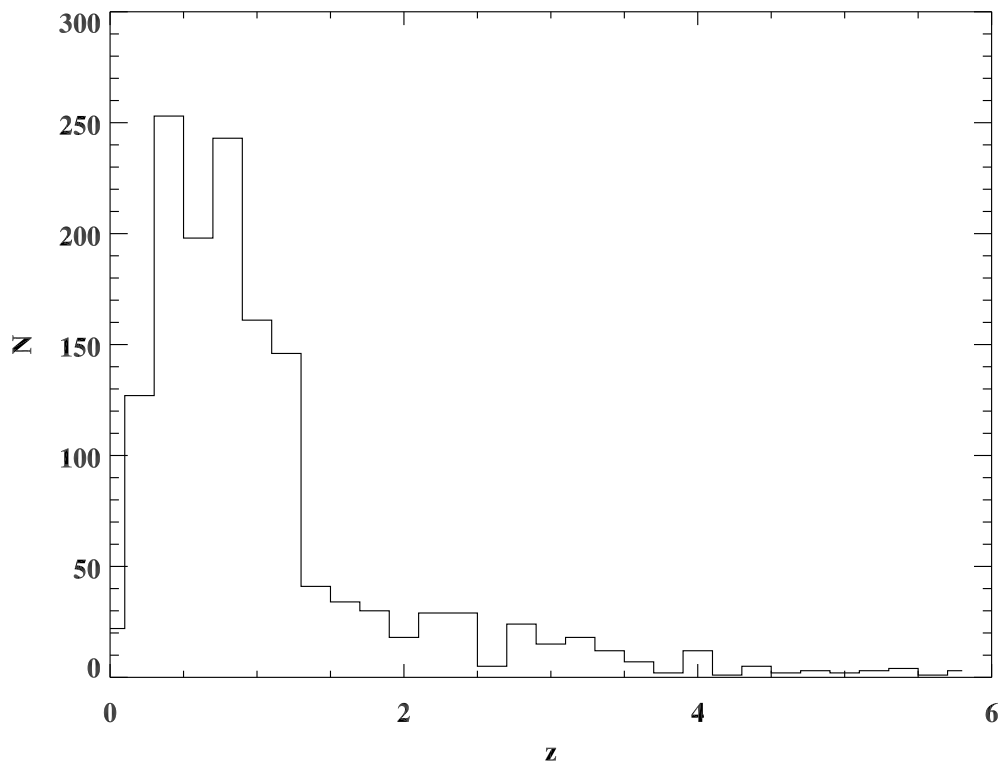


Fig. 1.— Histogram distribution of the spectroscopic redshifts of the total sample.

3. Surface Luminosity Priors

If we were to observe a galaxy with a standard intrinsic luminosity per unit area (hereafter denoted as I) at different redshifts, its measured surface brightness would go down as $I \propto (1+z)^{-4}$. Due to the limitation of the available photometry in wavelength less than 10,000 Å, we choose the rest-frame SL in B band, I_B , as prior probability, with redshifts extending to $z \sim 2.0$. The adoption of rest-frame B band is more sensitive to galaxy types from starbursts, spirals to ellipticals than redder bands. The intrinsic evolution of galaxy type with redshift and the observation selection effect will make the relation deviate from power -4 and we will calibrate this relation first. A subsample of 283 elliptical galaxies (Ferrerias et al. 2009) is used to examine the difference of the relation between the SL and redshift galaxy types. For galaxies with redshifts $z \lesssim 0.33$ we measure the SL I_B in the band closest to B : the V band magnitude for galaxies at redshift $0.33 \lesssim z \lesssim 0.96$, the i band for $0.96 \lesssim z \lesssim 1.35$, and the z band for $1.35 \lesssim z \lesssim 2.0$.

The photometry of GOODS version 2.0 catalog is measured in AB magnitudes (Oke & Gunn 1983), which are defined as:

$$m = -2.5 \log f_\nu - 48.6, \quad (1)$$

where f_ν is the flux per unit frequency in unit of $\text{erg s}^{-1} \text{cm}^{-2} \text{Hz}^{-1}$. The half-light radii are measured by SExtractor and translated into angular radius, r_e (in arcsecond), by multiplying with the pixel scale $0''.03 \text{pix}^{-1}$. With the flux f_ν and half-light radius r_e in the corresponding band for different redshift range galaxies, the rest-frame B -band SL is calculated as follows

$$I_B = \frac{\Delta\nu_B f_\nu 4\pi d_L^2}{(1+z) 2\pi d_A^2 r_e^2} = \frac{2\Delta\nu_B f_\nu (1+z)^3}{r_e^2}, \quad (2)$$

where z is the redshift of galaxy, $\Delta\nu_B$ is the frequency interval corresponding to the wavelength range in the B band, f_ν is the flux in the observed filter band, d_L is luminosity distance and d_A is angular distance of galaxy, and I_B is SL in luminosity per unit area (in L_\odot/kpc^2). Figure 2 shows the distribution of the rest-frame B -band surface brightness with redshift for the spectroscopic galaxies. The range of I_B goes approximately from 10^6 to $10^{10} L_\odot/\text{kpc}^2$. The upper and lower limits of the observed surface brightness in magnitude per square arcsecond, $22.3 \text{ mag/arcsec}^2$ and $26.3 \text{ mag/arcsec}^2$ (corresponding to the magnitude range from 21 to 25 mag), are plotted as dotted lines in the figure. The relation between $\log I_B$ and $\log(1+z)$ is fitted linearly, which goes as $\log I_B = 2.61(\pm 0.06) \cdot \log(1+z) + 6.64(\pm 0.01)$. The triangular points in the figure represents the elliptical galaxies in our sample. The redshifts of ellipticals range from 0.3 to 1.4. The ellipticals show generally higher surface luminosities than blue galaxies while a much similar slope of $2.90(\pm 0.6)$. Compared with that found in Stabenau et al. (2008), for passively evolving red galaxies, the observed surface

brightness is close to $(1+z)^{-4}$, and the blue galaxies have a shallower slope, we do not find relatively flatter slope of the rest-frame SL for early-type galaxies here, and it may be due to the relatively small number of the sample. The final results show that there is little difference of the improvement in redshift estimation accuracy for red galaxies and blue galaxies.

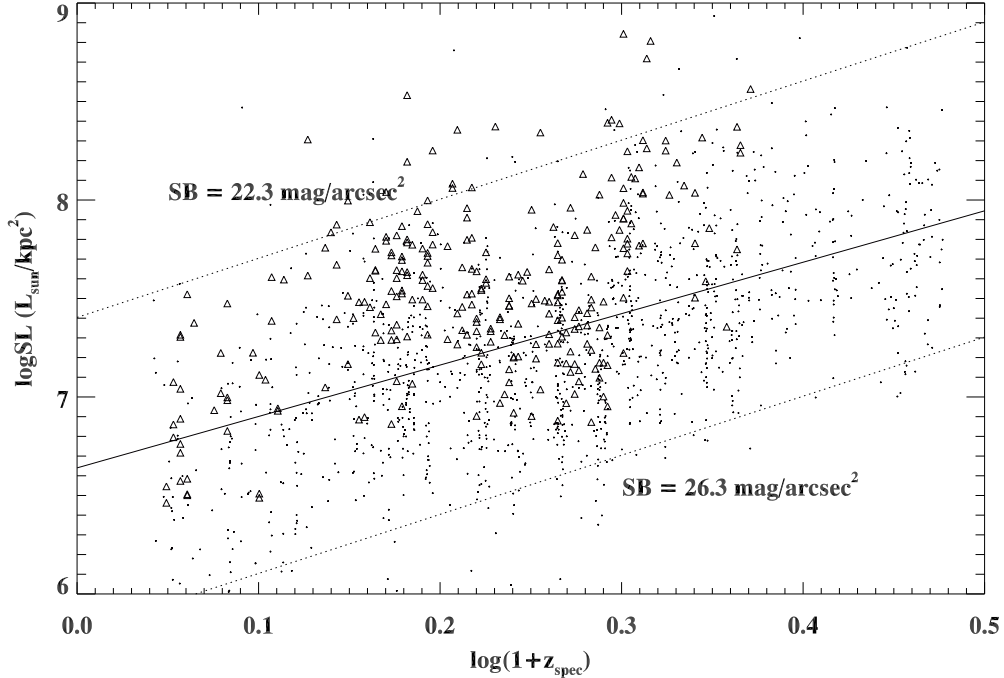


Fig. 2.— Distribution of rest-frame B -band SL I_B as a function of redshift for the total sample. The triangular points represent elliptical galaxies in our sample. The upper and lower limits of the observed surface brightness, 22.3 and 26.3 mag/arcsec $^{-2}$, are plotted as dotted lines. The points shows a good linear relation, $\log I_B \sim 2.61 \cdot \log(1+z)$, between SL and redshift. The ellipticals have a similar slope of 2.90.

To apply the scaling of SL with redshift as prior probability, we use a color-shape (Koo 1985) parameter $(B-V) - (i-z)$ to divide the sample into subsamples. Figure 3 plots the distribution of $(B-V) - (i-z)$ with redshift. We can see that this shape parameter declines linearly with redshift at $z \lesssim 1.3$ and it increases linearly with redshift at $z \gtrsim 1.3$. This is because that the shape parameter traces the position of 4000 Å break. Three subsamples are obtained with $(B-V) - (i-z) > 0.65$, $0 < (B-V) - (i-z) < 0.65$, and $(B-V) - (i-z) < 0$, corresponding to galaxies in redshift bins of $z \lesssim 1.0$, $0.6 \lesssim z \lesssim 1.2$, and $z \gtrsim 1.0$. The surface luminosity distribution is fitted by Gaussian functions for the three subsamples. The

distribution of $\log I_B$ with redshift and the Gaussian fits are plotted in Figure 4. The peak value of the Gaussian distribution slightly increases from $\log I_{B,0} = 7.02, 7.03$ to 7.30 with 1σ width of $0.48, 0.49,$ and 0.44 for the three subsamples, respectively.

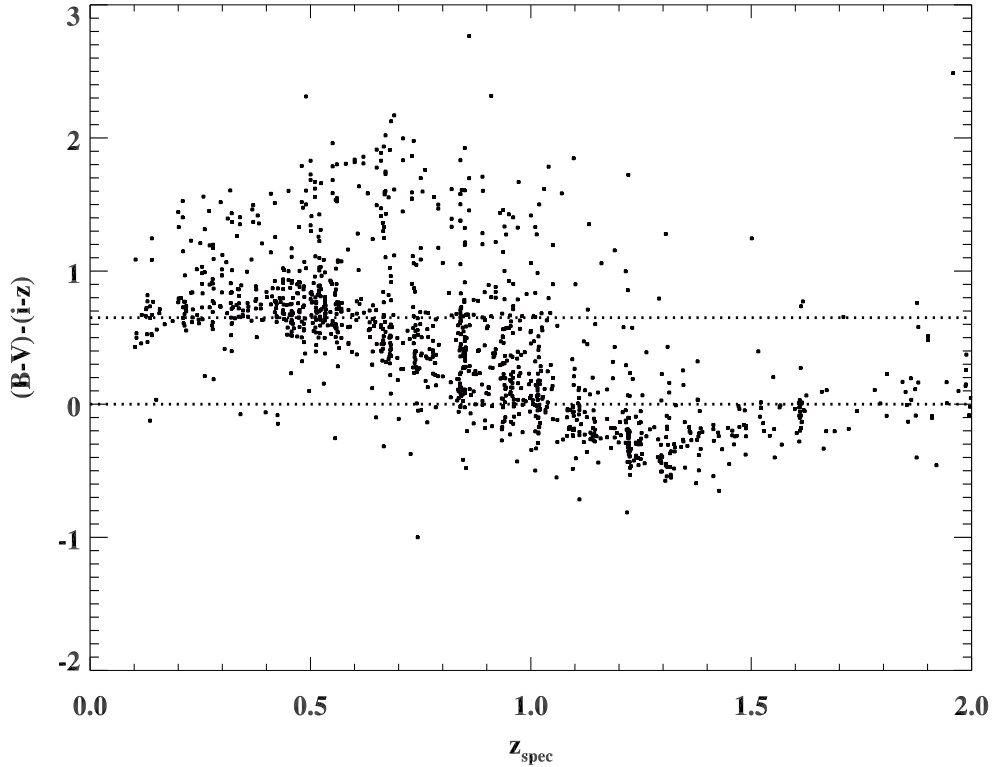


Fig. 3.— Distribution of color-shape parameter $(B - V) - (i - z)$ with redshift z for the spectroscopic galaxies. The dotted lines represent the criteria of $(B - V) - (i - z) > 0.65$, $0 < (B - V) - (i - z) < 0.65$ and $(B - V) - (i - z) < 0$, which are implemented to divide sample into three redshift bin subsamples.

The SL prior probability is calculated with the formula as

$$p(z|I_B(z)) = \frac{\phi}{\sqrt{2\pi}\sigma} \exp\left(\frac{-(\log I_B(z) - \log I_{B,0})^2}{2\sigma^2}\right), \quad (3)$$

where ϕ is the normalization constant so that the integration of the probability in the studied redshift range ($0 < z < 7$) is 1, σ is the width of the Gaussian profile, and $\log I_{B,0}$ is the Gaussian peak value. $I_B(z)$ is the surface brightness for one galaxy at different redshifts, calculated over a redshift range $0.10 < z < 7.0$ with a step of 0.005 , the same as that of SPZs.

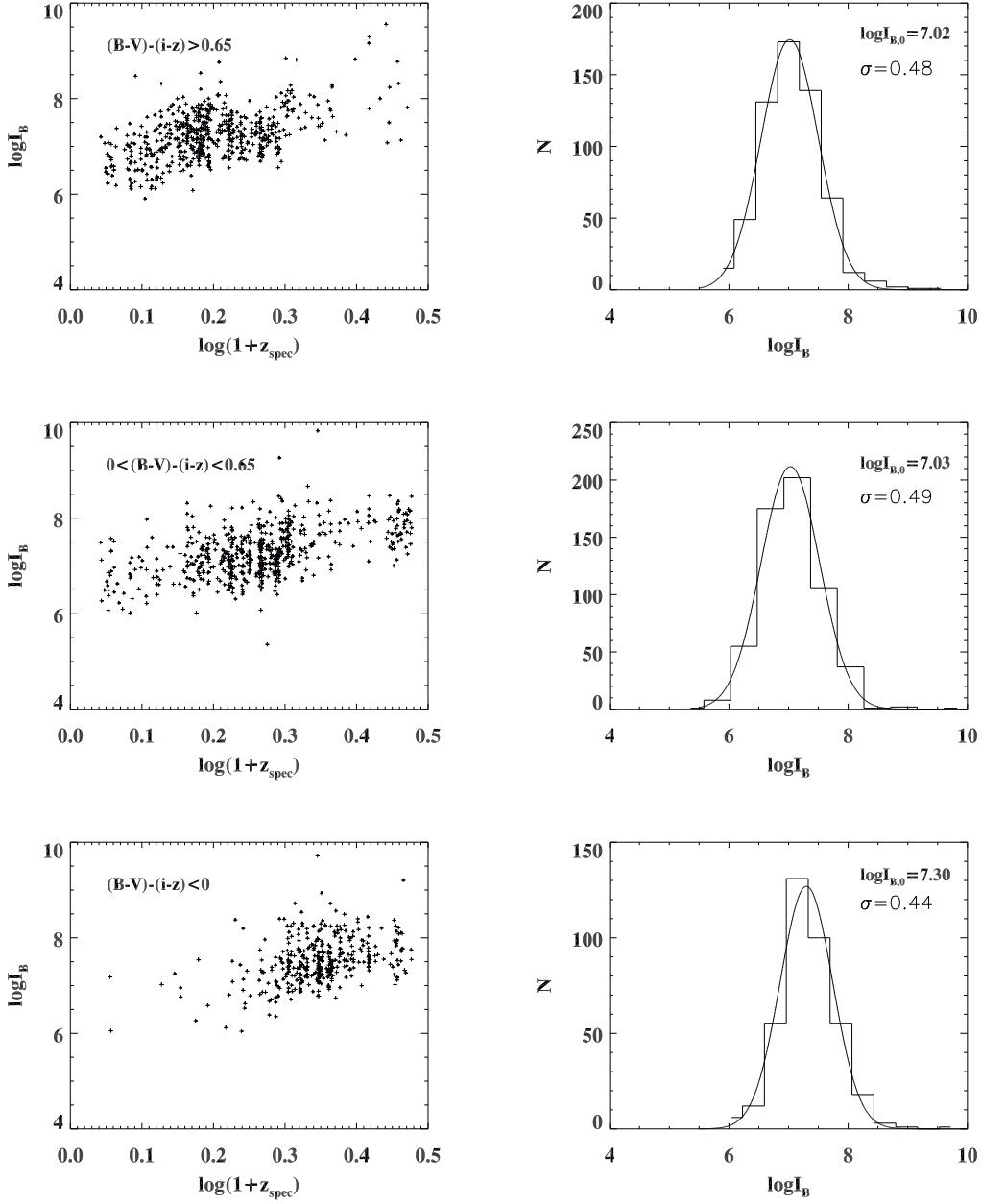


Fig. 4.— Distribution of $\log I_B$ with redshift and the Gaussian fitting for the three color-shape parameter divided subsamples. Left panel: from top to bottom, the three subsamples have $(B - V) - (i - z) < 0.65$, $0 < (B - V) - (i - z) < 0.65$ and $(B - V) - (i - z) < 0$, respectively. Right panel: the distribution of $\log I_B$ is fitted by a Gaussian function. The peak and the width of the Gaussian distributions are $\log I_{B,0} = 7.02, 7.03, 7.30$ and $\sigma = 0.48, 0.49, 0.44$ for the three subsamples, respectively.

The best redshift is estimated by the combination of SL prior probabilities and SPZ fitting probabilities, which are output from *HyperZ*. Using Bayes’ theorem, the final probability of redshift can be computed as

$$p(z|I_B(z), C) = \frac{p(z|I_B(z)) \times p(C|z)}{p(C)}, \quad (4)$$

where $p(z|I_B(z))$ is the redshift probability given by SL priors, and $p(C|z)$, $P(C|z) = \exp(-\chi^2(z)/2)$, is the probability of the galaxy at redshift z with the observed color C given by the SPZs estimation.

4. Implication and Results

For the 1266 galaxies, we first divide galaxies into subsamples by the color-shape parameter. Then we calculate the SL prior probability for galaxies by the corresponding Gaussian profiles in different subsamples. Combining the SL prior probability with the SPZ likelihood function, we obtain the best redshift as the maximum of the final probability distribution.

Figure 5 shows four examples of redshift probability distributions for galaxies in GOODS-N field. The ID of the object is labeled at the right-bottom of the panel. The dashed line in the figure represents the likelihood function given by SPZ SED fitting. The dotted line represents the calculated probabilities by SL priors. The solid line shows the combined probability distribution from SPZ SED fitting and SL priors. The vertical dash-dotted line represents the position of the spectroscopic redshift. The upper-left panel shows a case where the SPZ redshift estimation gives two peaks in the redshift probability function. The addition of the SL priors probability gives the correct distribution around the spectroscopic redshift. With the combination of the two probabilities, the correct peak is chosen, and the probability of a catastrophic redshift estimation is reduced. The upper-right panel shows an example where the SPZ does not produce a reasonable likelihood distribution, though the SL priors give more reasonable estimation. The lower-left panel gives an example of the correct estimation of redshift by both methods. In the lower-right panel, the SL priors choose the wrong peak of the SPZ $p(z)$ distribution for a galaxy with redshift $z = 1.6$. This can be the reason of the larger deviation of redshift estimation with SL priors at redshift $z > 1.6$. The results of redshift estimation with SL priors are shown in Figure 6.

Figure 6 shows the comparison of SPZs with and without SL priors. The upper two panels in Figure 6 show the comparison between SPZ redshifts and spectroscopic redshifts, and the distribution of redshift fractional error $\Delta(z) = \frac{\Delta z}{1+z}$ with spectroscopic redshifts. The triangular points in figure are galaxies in the GOODS-S field which are supplemented with

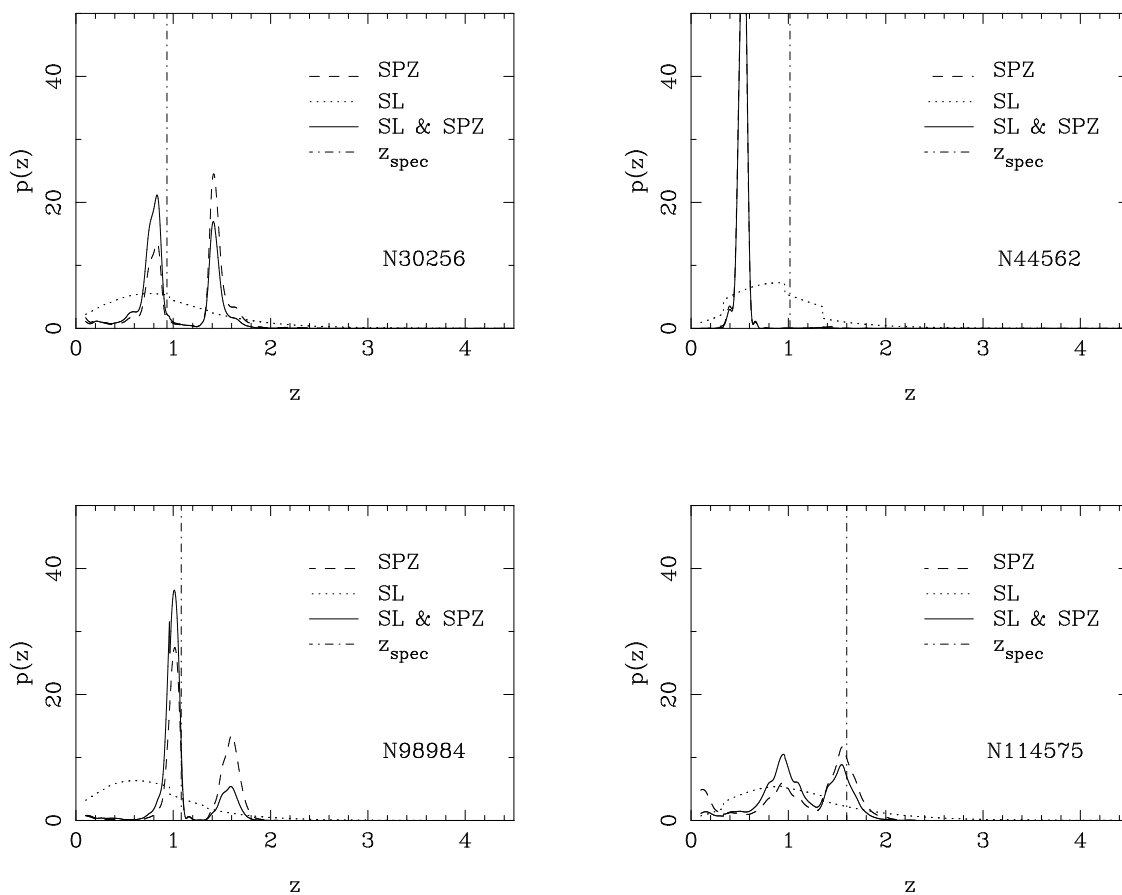


Fig. 5.— Probability distributions as a function of redshift obtained from the SPZ SED fitting, the SL priors, and the combination of SPZ SED fitting with SL priors. The dashed line represents the likelihood function given by SPZ SED fitting. The dotted line represents the calculated probabilities by SL priors. The solid line shows the combined probability distribution. The vertical dash-dotted line represents the position of the spectroscopic redshift. The object ID is labeled at the right-bottom in the panel.

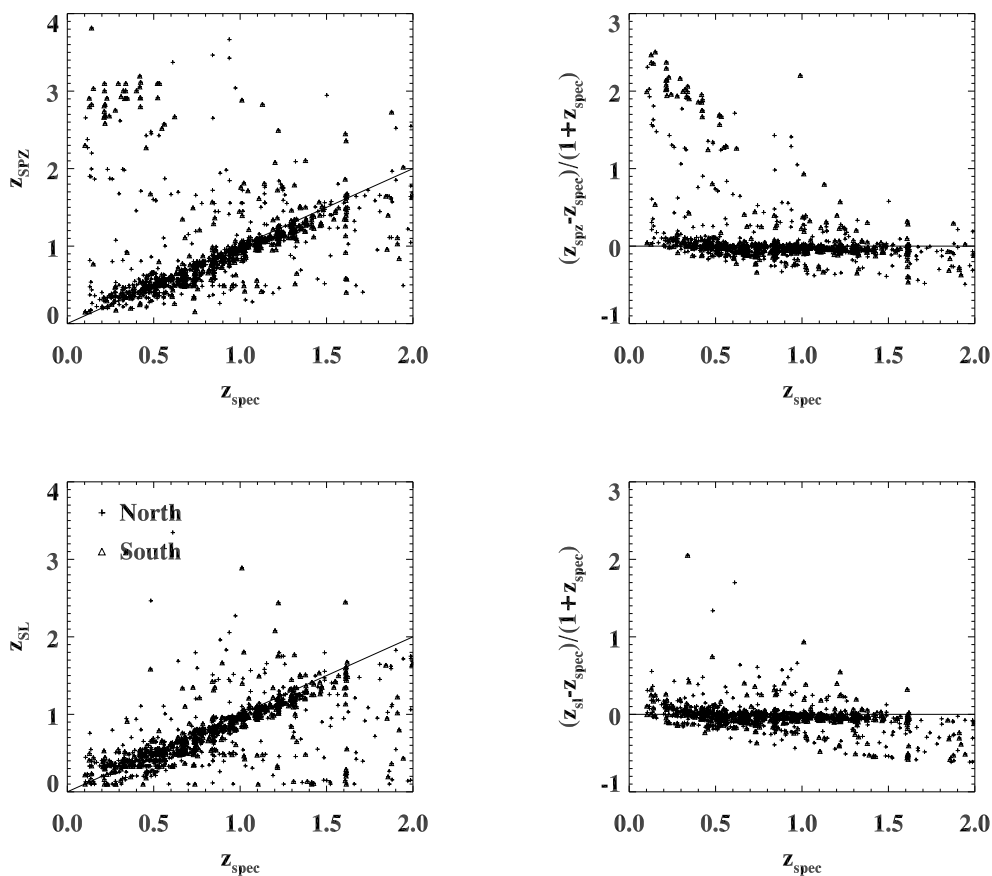


Fig. 6.— Left panels show the comparison between estimated redshifts and spectroscopic redshifts. The upper one is the comparison between SPZ redshifts and spectroscopic redshifts. The lower one is that of the improved SPZ redshifts by SL priors. The cross points illustrate the galaxies in GOODS-N field; the triangular points are galaxies in GOODS-S field. The right panels show the distribution of the fractional error $\Delta(z)$ with redshift for the redshift estimation with and without SL priors.

infrared JHK photometry, and the cross dots are galaxies in the GOODS-N field, which have U -band data. From this comparison, we can see that many galaxies in the GOODS-S field with $z < 0.6$ are estimated to be around $z \simeq 2\text{--}3$ by the SPZ method. Because the 4000 Å break of $z < 0.6$ galaxies falls in the UV/B band, it can be confused with galaxies of $z \sim 3.0$ with the Lyman break falling in B/V band. From this comparison, we can also see that the scatter improves greatly for galaxies in GOODS-N field. The GOODS-N field has fewer catastrophic outliers because of U -band photometry for galaxies.

The bottom two panels show the results of the photometric redshifts with SL prior probabilities. From the comparison of the redshift estimation with and without SL priors, the effectiveness of SL priors is illustrated in breaking the redshift degeneracy, and in reducing the fraction of catastrophic outliers. For the total sample at $0.1 \lesssim z \lesssim 2.0$, the accuracy of the redshift estimation by SL priors (which is the width of the Gaussian error distribution) changes little from $\sigma(\Delta(z)) = 0.043$ with an systematic offset of -0.019 to $\sigma(\Delta(z)) = 0.044$ with an offset of -0.020 . We can see from the figure that at redshifts $z \lesssim 0.3$ and $z \gtrsim 1.6$, the SL priors do not work as well as in the intermediate redshift range. This is because the peak value of the SL sampled by the SL priors is slightly larger than the actual SL for galaxies with lower redshifts, and is slightly smaller than the actual SL for the galaxies with highest redshifts. For galaxies in the redshift range $0.5 \lesssim z \lesssim 1.25$, the rms error remains the same at $\sigma_x = 0.035$ for both methods. For galaxies with redshift $z > 1.6$, the SPZ yields large scatter. We only use the 1183 galaxies at $z < 1.6$ to calculate the statistics of catastrophic outliers. For galaxies with $|\Delta(z)| > 0.2$, the fraction decreases from 15.0% to 10.4% by adding SL priors; and for galaxies with $|\Delta(z)| > 0.5$, the number reduces from 87 to 22. This effect is demonstrated clearly in Figure 7, which shows the histogram of the fractional redshift error. The solid line shows the histogram of galaxies with improved SPZ redshifts by SL priors. The dotted line represents that of galaxies with SPZ redshifts. We can see that the galaxies with fractional errors greater than 0.6 almost disappear with the SL priors method.

For the 283 elliptical galaxies, the redshift estimation shows same trend as that of the total sample, with little change in accuracy and improvement in catastrophic outliers. The redshift accuracy is $\sigma(\Delta(z)) \sim 0.01$, much better than that of the blue galaxies, for both SPZs and SPZs with SL priors. The elliptical galaxies in the spectroscopic sample is not complete due to the selection effects and it can lead to small difference in the accuracy estimation. In the application to the photometric sample with this calibration, there is type selection bias in different redshifts. At higher redshifts, the photometric sample tends to have more luminous elliptical galaxies, which should have better accuracy in redshift estimation.

The color and SL priors works well for lower redshift samples at $z \lesssim 1.6$. However, to

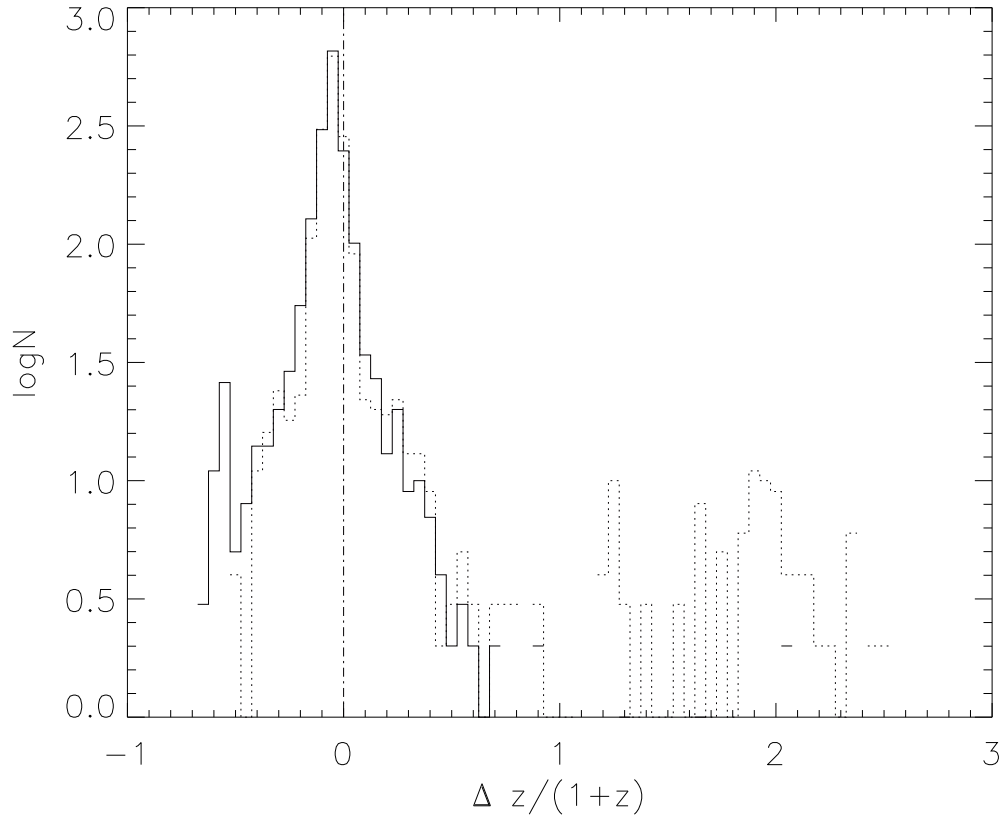


Fig. 7.— Histogram distribution of redshift fractional error x . The solid line shows the improved SPZ redshifts by SL priors. The dotted line represents the distribution of SPZ redshifts. The dash-dotted line shows the zero position of the histogram.

apply this method to redshift estimation for the whole PEARS sample, we need to improve the method, since the whole sample will include such galaxies at $z \gtrsim 1.6$ and the relation between the shape parameter $(B - V) - (i - z)$ and redshift will not be near linear. The value of $(B - V) - (i - z)$ will go up linearly with redshift at $z \gtrsim 1.6$. The application of this method needs to be studied further, likely with additional near-IR filters to obtain the photometry of rest-frame B -band. This can be done with the *HST*/WFC3 after 2009.

5. Summary and Conclusions

For an object with constant luminosity per unit area, the bolometric surface brightness scales as $(1 + z)^{-4}$ in an expanding universe. That, combined with the fact that there is a definite upper limit to luminosity per unit area seen in starburst galaxies from $z = 0-7$ (Hathi et al. 2008; Meurer et al. 1997), would make for a very strong prior for photometric estimates. However, the mean luminosity per unit area is well below this upper limit and shows strong redshift evolution for blue late-type galaxies. The early-type galaxies show a generally higher SL and a similar slope of the redshift evolution.

To calibrate the evolution of luminosity per unit area, we divide the sample into three redshift bins using a color-based criterion; and then derive the distribution of luminosity per unit area in rest-frame B band. The probability of the rest-frame SL is applied as a prior to the redshift probabilities given by SED fitting to broadband + grism data.

The method is applied to 1266 galaxies observed with *HST*/ACS PEARS grism spectra and with GOODS *BViz* broadband photometry and known ground-based redshifts in the range of $0.1 \lesssim z \lesssim 2.0$. The accuracy is assessed with the spectroscopic redshifts. By comparing the redshift estimation with and without SL priors, the new method improves the number of galaxies with $|\Delta(z)| > 0.2$ from 15.0% to 10.4%. The rms scatter does not change much. The improvement seems same for the blue galaxies and the 283 red galaxies, while the red galaxies show higher accuracy in redshift estimation. The result shows the efficiency of the SL priors in breaking the degeneracy of SPZ redshifts for low-redshift Balmer break galaxies and high-redshift Lyman break galaxies.

PEARS is an HST Treasury Program 10530 (S. Malhotra, PI). Support for program was provided by NASA through a grant from the Space Telescope Science Institute, which is operated by the Association of Universities for Research in Astronomy, Inc., under NASA contract NASA5-26555 and is supported by HST grant 10530.

REFERENCES

- Baum, W. A. 1962, IAU Symp. 15, Problems of Extra-Galactic Research, ed. G. C. McVittie (New York: Macmillan), 390
- Benítez, N. 2000, ApJ, 536, 571
- Blanton, M. R. et al. 2003, AJ, 125, 2348
- Bolzonella, M., Miralles, J.-M., & Pelló, R. 2000, A&A, 363, 476
- Budavári, T., Szalay, A. S., Connolly, A. J., Csabai, I., Dickinson, M. E., & the HDF/Nicmos Team 1999, ASP Conf. Ser, 191, Photometric Redshifts and High Redshift Galaxies, ed. R. J. Weymann, L. J. Storrie-Lombardi, M. Sawicki, & R. Brunner (San Francisco: ASP), 19
- Budavári, T., Szalay, A. S., Connolly, A. J., Csabai, I., & Dickinson, M. E. 2000, AJ, 120, 1588
- Budavári, T., et al. 2001, AJ, 121, 1163
- Capak et al. 2004, AJ, 127, 180
- Cohen, S. et al. 2009, AAS, 21342426, in preparation
- Connolly, A. J., Csabai, I., Szalay, A. S., Koo, D. C., Kron, R. G., & Munn, J. A. 1995, AJ, 110, 2655
- Csabai, I., Connolly, A. J., Szalay, A. S., & Budavari, T. 2000, AJ, 119, 69
- Fernández-Soto, A., Lanzetta, K. M., Yahil, A. 1999, ApJ, 513, 34
- Ferreras, I. et al. 2009, MNRAS, 395, 554
- Ford, H. C., Clampin, M., Hartig, G. F., et al. 2003, SPIE, 4854, 81
- Giavalisco, M., et al. 2004, ApJ, 600, 93
- Grazian, A., et al. 2006, A&A, 449, 951
- Hathi, N. P., Malhotra, S., & Rhoads, J. E. 2008, ApJ, 673, 686
- Hickson, P., Gibson, B. K., & Callaghan, K. A. S. 1994, MNRAS, 267, 911
- Komatsu et al. 2009, ApJS, 180, 330

- Koo, D. C. 1985, *AJ*, 90, 418
- Koo, D. C. 1999, *ASPC*, 191, *Photometric Redshifts and High Redshift Galaxies*, ed. R. J. Weymann, L. J. Storrie-Lombardi, M. Sawicki, & R. Brunner (San Francisco: ASP), 3
- Kurtz, M. J., Geller, M. J., Fabricant, D. G., Wyatt, W. F., & Dell Antonio, I. P. 2007, *AJ*, 134, 1360
- Mobasher, B., et al. 2004, *ApJ*, 600, 167
- Mobasher, B., et al. 2007, *ApJ*, 172, 117
- Meurer, G. R., Heckman, T. M., Lehnert, M. D., Leitherer, C., & Lowenthal, J. 1997, *AJ*, 114, 54
- Oke, J. B., & Gunn, J. E. 1983, *ApJ*, 266, 713
- Pahre, M. A., Djorgovski, S. G., & de Carvalho, R. R. 1996, *ApJ*, 456, 79
- Pirzkal, et al. 2004, *APJS*, 154, 501
- Retzlaff, J. et al. 2009, in preparation
- Ryan, R. et al. 2007, *ApJ*, 668, 839
- Sandage, A., & Lubin, L. M. 2001, *AJ*, 121, 2271
- Stabenau H. F., Connolly, A., Jain, B. 2008, *MNRAS*, 387, 1215
- Tolman, R. C. 1930, *Proc. Natl. Acad. Sci.*, 16, 511
- Vanzella, E., et al. 2008, *A&A*, 478, 83
- Wang, Y., Bahcall, N., & Turner, E. L. 1999, *AJ*, 116, 2081
- Wirth, G. D., et al. 2004, *AJ*, 127, 3121
- Wray, J. J., Gunn, J. E. 2008, *ApJ*, 678, 144
- Wolf, C. et al. 2001, *A&A*, 365, 681
- Wolf, C. et al. 2003, *A&A*, 401, 73
- Xia, L., et al. 2002, *PASP*, 114, 1349

Zhou, X., Jiang, Z. J., Xue, S. J., Wu, H., Ma, J., & Chen, J. S. 2001, *Chin. J. Astron. & Astrophys.*, 1, 372